Qiu *et al.*
EURASIP Journal on Advances in Signal Processing (2022) 2022:22
https://doi.org/10.1186/s13634-022-00856-5

EURASIP Journal on Advances in Signal Processing

RESEARCH Open Access

An improved local oscillator modulation of modulated sampling scheme for multiple mono-pulse radar signals reconstruction

Zhaoyang Qiu[1], Minhong Sun[1*], Jun Zhu[2], Xuyang Teng[1] and Huina Song[1]

*Correspondence: cougar@hdu.edu.cn
[1] School of Communication Engineering, Hangzhou Dianzi University, Hangzhou, People's Republic of China
Full list of author information is available at the end of the article

Abstract

The modulated sampling scheme can intercept noncooperative signals distributed in a wide frequency band by using a single receiving channel, which is an efficient architecture in many radar and communication applications. The modulated sampling scheme employs a non-uniform sample pulse train to fold the intercepted signal prior to quantization/digitization by using a local oscillator (LO) that contains a certain modulation type. Since the mono-pulse radar signals are widely used in many radar systems, the modulated sampling scheme will receive the multiple mono-pulse radar signals simultaneously in dense signal environment, and the folded outputs of the modulated sampling scheme may meet frequency aliasing. Thus, it is necessary to investigate the reconstruction of the multiple mono-pulse signals intercepted by the modulated sampling scheme in the frequency aliasing situation. In this paper, based on the orthogonal matching pursuit algorithm, the LO modulation type of the modulated sampling scheme is analyzed to achieve a better reconstruction performance of the multiple mono-pulse signals. The drawback of the typical LO using sinusoidal frequency modulation to reconstruct multiple mono-pulse signals is investigated firstly. Then, an improved LO using periodic linear frequency modulation is proposed, and its effectiveness to reconstruct multiple mono-pulse signals is analyzed. Furthermore, the parameter setting criterion of the improved LO modulation is given, and the comparison using other modulation types is discussed. Finally, several simulations are conducted to prove our analysis and the improved LO modulation can reconstruct multiple mono-pulse signals under the frequency aliasing condition.

Keywords: Modulated sampling scheme, Multiple mono-pulse signals, Local oscillator modulation, Signal reconstruction, Orthogonal matching pursuit algorithm

1 Introduction

Presently, the noncooperative receiver in many applications requires a wide receiving bandwidth to achieve a high interception probability [1, 2]. However, the typical noncooperative receiver using uniform sampling based on direct Nyquist rate digitalization is difficult to realize the wideband receiving because of the analog-to-digital converter (ADC) sample rate limitation [3].

In recent years, several sampling theories are proposed to overcome the ADC limitations, such as the sample rate and the saturation [4, 5]. In the field of sample rate, the analog-to-information (A-to-I) theory is a novel approach to break the ADC sample rate limitation [6]. For instance, the random sampling scheme based on the compressive sensing (CS) is a typical A-to-I theory, and several wideband CS receiving structures are designed [7, 8]. Besides, the signal recovery and processing methods based on the corresponding schemes are proposed [9, 10]. Then, another A-to-I method named as the modulated sampling scheme is proposed, and the Nyquist folding receiver (NYFR) is designed based on this scheme [11, 12]. Compared with random sampling scheme or the modulated wideband converter (MWC) using multiple clocks [7], the modulated sampling scheme only requires a single channel to achieve wideband receiving and it preserves the signal structure [12], which means the receiving resource of the modulated sampling scheme is low and its output can be processed easier. Based on the modulated sampling scheme, the improved NYFR structures, the output characteristics and the corresponding signal processing are investigated [13–17]. The modulated sampling scheme uses a non-uniform modulated radio frequency (RF) sampling to realize wideband receiving. The RF sampling is controlled by a local oscillator (LO) that contains a certain modulation type, and the non-uniform sample pulse train is generated by the LO. Usually, the typical LO modulation type of the modulated sampling scheme is sinusoidal frequency modulation (SFM) [12]. The intercepted signal with a high frequency in the wide frequency space is converted to a low frequency by mixing process using the non-uniform sample pulse train. The folded signal contains the bandwidth of the LO modulation, and this bandwidth is the information to recover the original frequency of the intercepted signal [12, 13].

Meanwhile, the mono-pulse signal has been widely used in many radar systems [18], and the wideband receiver will intercept the multiple mono-pulse radar signals in dense signal environment. In the noncooperative receiving applications, the intercepted radar signals are unknown, and these unknown signals are required to be reconstructed to obtain their information [3]. Because the modulated sampling scheme can be applied to intercept the multiple mono-pulse radar signals in the wide frequency space, it is required to have the ability for multiple mono-pulse signals recovery [17]. Currently, the main existing studies of the modulated sampling focus on the information recovery and the single signal reconstruction in the view of signal processing [19, 20]. When the multiple mono-pulse signals are intercepted by the modulated sampling scheme, the folded outputs will meet frequency aliasing, and it is necessary to analyze the reconstruction of the multiple mono-pulse signals. Because the typical modulated sampling scheme using the SFM LO may fail to reconstruct the multiple mono-pulse signals [17], this paper will analyze the relation between the LO modulation type and the reconstruction of the multiple mono-pulse signals in the view of the receiving architecture and propose a new LO modulation type to obtain a better reconstruction performance. The modulated sampling is in the middle of the uniform sampling and the CS random sampling, and the CS model of the modulated sampling can be employed to analyze this scheme [11]. Because the orthogonal matching pursuit (OMP) algorithm is a general reconstruction approach based on the CS model [11, 12], it is chosen as the reconstruction method in this paper.

The main contributions of this paper are as follows. Firstly, considering the completely frequency aliasing condition and based on the modulated sampling scheme using the typical LO modulation, the failure reason of the OMP algorithm to reconstruct multiple mono-pulse radar signals in wideband frequency space is analyzed mathematically. Secondly, an improved LO modulation type is proposed, which can reconstruct the multiple mono-pulse signals intercepted by the modulated sampling scheme in the completely frequency aliasing situation. In addition, the parameter setting criterion of the improved LO modulation and the comparison with other modulations are discussed.

This paper is organized as follows: Section 2 gives the signal model and the modulated sampling scheme CS model. In Sect. 3, the typical LO modulation using the SFM and the multiple mono-pulse signals reconstruction are analyzed based on the OMP algorithm. Specifically, reconstruction failure reason under the completely frequency aliasing condition is investigated. In Sect. 4, the improved LO modulation type is proposed, which can reconstruct the multiple mono-pulse signals in the completely frequency aliasing situation. Meanwhile, its parameter setting criterion and the comparison with other different LO modulations are discussed. The simulations are demonstrated and analyzed in Sect. 5. The results' discussion of this paper and the conclusion are given in Sect. 6 and Sect. 7, respectively.

2 Mathematical model

The multiple simultaneous intercepted complex mono-pulse radar signals can be written as:

$$x(t) = \sum_{i=1}^{s} A_i e^{2j\pi f_i t + j\varphi_i} \tag{1}$$

where s is the signal number, A_i, $i = 1, 2, \ldots, s$ is the amplitude of each signal, φ_i is the initial phase and f_i is the carrier frequency of each signal. In (1), $t \in [0,\ T)$, T is the signal time width in the observation window that can be obtained by the signal detection [21]. To simplify the following analysis, the initial phases are $\varphi_i = 0$. In the noncooperative receiving applications, the signals in (1) are unknown and carrier frequencies f_i in (1) are required to be obtained. For instance, the radar reconnaissance receiver intercepts the unknown signals in wide frequency space and it is a typical noncooperative receiver. Since the frequency aliasing situation is considered in this paper, the amplitudes in (1) are assumed as $A_i = A$, which implies the frequency aliasing is under the worst condition [9].

The modulated sampling scheme or the NYFR is given in Fig. 1 [11–13].

In Fig. 1, the LO carrier frequency is f_s and the Nyquist zone (NZ) bandwidth equals f_s when the input signals are complex [13]. The wideband RF filter allows several NZs to be sampled. The multiple input signals are mixed with the non-uniform sample pulse train after they are filtered by the wideband RF filter. The non-uniform sample pulse train is generated by the LO and each sample times t_k is at the zero-crossing rising (ZCR) time of the RF sample clock. Because the RF sample clock contains a modulation $\theta(t)$, the sample pulse train is non-uniform, and the average sample rate of the non-uniform sample pulse train is f_s. The mixed signals in the 0^{th} NZ are filtered by a normalized interpolation filter whose

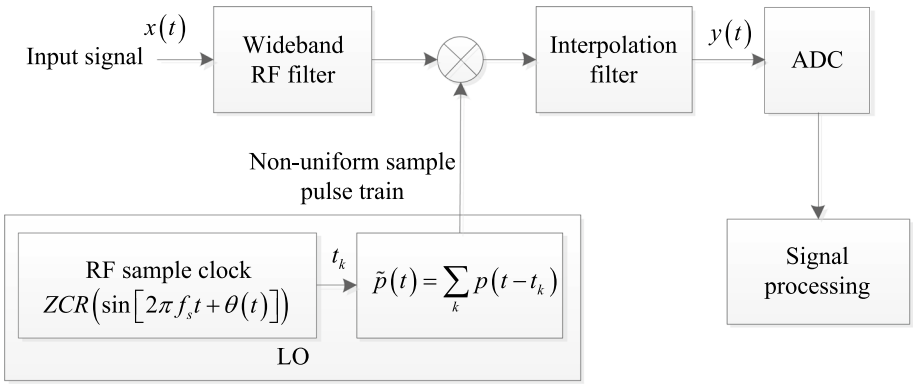

Fig. 1 Modulated sampling scheme

pass band is f_s. At last, the filtered signal $y(t)$ is sampled again by an ADC with a low sample rate that satisfies the Nyquist sampling theorem.

Considering the noncooperative receiving, the signal with a high carrier frequency is hard to be directly sampled because of the ADC sample rate limitation. The modulated sampling scheme can fold the signal with high carrier frequency to the low frequency by the mixing process of the non-uniform sampling in Fig. 1, and it realizes the wideband receiving by an ADC with a low sample rate. The reconstruction means recovering the intercepted signal by using the modulated sampling scheme and the folded output [11, 12].

Then, the model of the modulated sampling scheme is given. The multiple intercepted mono-pulse signals in frequency domain are $\mathbf{X} = \mathcal{F}[x(t)]$, where $\mathcal{F}$ is the Fourier transform operator. Since the spectra of the intercepted signals can be represented as a Nyquist rate sampled vector and considering the CS theory, the input $\mathbf{X} \in \mathbb{C}^N$ is an s-sparse vector and the output is $\mathbf{y} \in \mathbb{C}^M$[12, 22], where $N = MK$, K is the number of NZs, M is the element number of $\mathbf{y}$ and N is the element number of $\mathbf{X}$. Hence, the modulated sampling scheme in Fig. 1 can be modeled as [12]

$$\mathbf{y} = \Phi\mathbf{X} \tag{2}$$

where $\mathbf{\Phi} \in \mathbb{C}^{M\times N}$ is the sensing matrix, $\mathbf{X} = [X_0, X_1, \cdots, X_{M-1}, \cdots, X_{N-1}]^T$ is the input in frequency domain, and $\mathbf{y} = [y_0, y_1, \cdots, y_{M-1}]^T$ is the output in time domain.

Based on Fig. 1, the sensing matrix $\mathbf{\Phi}$ can be expressed as [12, 17]

$$\mathbf{\Phi} = \mathbf{RS}\Psi \tag{3}$$

In (3), we have

$$\mathbf{R} = \left[\, \mathbf{I}_M \;\; \mathbf{I}_M \;\; \cdots \;\; \mathbf{I}_M \,\right] \tag{4}$$

$\mathbf{I}_M$ is an $M \times M$ identity matrix in (4),

$$\mathbf{S} = \begin{bmatrix} \mathbf{I}_M & & & \\ & e^{-j\theta(m)}\mathbf{I}_M & & \\ & & \ddots & \\ & & & e^{-j(K-1)\theta(m)}\mathbf{I}_M \end{bmatrix} \tag{5}$$

where $m \in [0,\ M-1]$. The block diagonal matrix in (4) is

$$\mathbf{\Psi} = \begin{bmatrix} \boldsymbol{\psi}_M & & & \\ & \boldsymbol{\psi}_M & & \\ & & \ddots & \\ & & & \boldsymbol{\psi}_M \end{bmatrix} \tag{6}$$

where $\boldsymbol{\psi}_M \in \mathbb{C}^{M\times M}$ is the inverse discrete Fourier transform (IDFT) matrix. Considering the typical modulated sampling scheme, the LO modulation in (5) is the SFM and it can be written as [12, 13]

$$\theta(m) = m_f \sin\left(2\pi f_{LO} m T_{ADC}\right) \tag{7}$$

where f_{LO} is the LO modulation frequency, T_{ADC} is the sampling interval of the ADC in Fig. 1, m_f is the SFM modulation coefficient, and the IDFT matrix $\boldsymbol{\psi}_M$ in (6) is

$$\boldsymbol{\psi}_M = \frac{1}{\sqrt{M}} \begin{bmatrix} 1 & 1 & \cdots & 1 \\ 1 & \omega & \cdots & \omega^{M-1} \\ \vdots & \vdots & \ddots & \vdots \\ 1 & \omega^{M-1} & \cdots & \omega^{(M-1)(M-1)} \end{bmatrix} \tag{8}$$

where $\omega = e^{j\frac{2\pi}{M}}$. To simplify the following analysis, m_f is assumed as 1 since it is used to change the SFM bandwidth [17].

According to (3), (4), (5) and (6), the sensing matrix $\mathbf{\Phi}$ in (2) can be calculated as:

$$\mathbf{\Phi} = \begin{bmatrix} \boldsymbol{\psi}_M & e^{-j\theta(m)}\boldsymbol{\psi}_M & \cdots & e^{-j(K-1)\theta(m)}\boldsymbol{\psi}_M \end{bmatrix} \tag{9}$$

Considering the multiple mono-pulse signals in (1), the sampling scheme in Fig. 1 and the sensing matrix in (9), the outputs of the modulated sampling scheme in (2) can be computed as

$$y(m) = A\sum_{i=1}^{s} e^{2j\pi\left(f_i - k_i f_s\right)mT_{ADC} - jk_i \sin\left(2\pi f_{LO} m T_{ADC}\right)} \tag{10}$$

where $k_i = round\left(f_i/f_s\right) \subset \{0,\ 1,\ \cdots,\ K-1\}$ is the NZ index of the ith intercepted mono-pulse radar signal. Compared with the intercepted signals in (1), the carrier frequencies of the folded outputs in (10) are in the 0th NZ and they are $f_i - k_i f_s$. The outputs contain the added LO modulation and it is the SFM. Besides, the output amplitudes remain unchanged because of the normalized interpolation filter, and the modulation type has no effect on the output power and the dynamic range [23]. To further illustrate the multiple outputs in (10), Fig. 2 shows the multiple mono-pulse signals receiving process based on the modulated sampling scheme.

In Fig. 2, four mono-pulse signals are intercepted simultaneously and these signals are located in four different NZs. According to the modulated sampling scheme, each folded

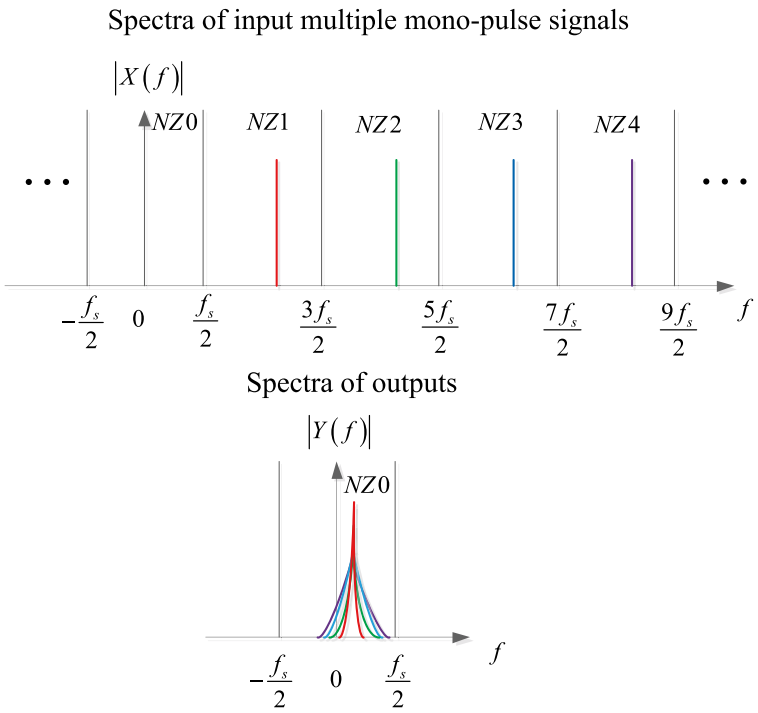

Fig. 2 Multiple mono-pulse signals receiving process based on modulated sampling scheme

signal is in the 0th NZ and it contains the LO modulation bandwidth, which is expressed in (10). The added bandwidth of each signal is different because the intercepted signals are located in different NZs. Particularly, when the folded carrier frequencies of the outputs $f_i - k_i f_s$ are the same, the spectra of outputs are completely frequency aliasing, and this situation is shown in Fig. 2. Because the signals intercepted by the noncooperative receiver are unknown, the frequency aliasing condition in Fig. 2 is inevitable. Therefore, the multiple signals reconstruction under the frequency aliasing condition is necessary to be considered. Since the characteristic of the output signal is decided by the LO, the LO modulation should be investigated to obtain a good reconstruction result.

3 Typical local oscillator modulation analysis

Generally, the typical LO modulation of the modulated sampling scheme is the SFM. Since the modulated sampling scheme can be expressed as the CS model in (2), the OMP algorithm is an effective method to reconstruct the intercepted signal [11, 12], and it is chosen as the reconstruction method in this paper. Before we start to analyze the relation between the LO modulation and the multiple signals reconstruction, the OMP algorithm based on the CS model in (2) is briefly given.

The steps of the OMP algorithm are as follows.

Step 1. Initialize: iteration counter $i_t = 0$, support set $\Lambda_0 = \emptyset$ and residual $\mathbf{r}_t = \mathbf{y}$, where $\mathbf{y}$ is the output in (2);

Step 2. Increment $i_t = i_t + 1$, and compute the atom $\varsigma_{i_t} = \underset{c=1,2,\cdots,N}{\arg\max} \left|\left\langle \mathbf{\Phi}_c, \mathbf{r}_{i_t-1} \right\rangle\right|$, where $\mathbf{\Phi}$ is the sensing matrix and c represents the column number of $\mathbf{\Phi}$;

Step 3. Update the support $\Lambda_{i_t} = \Lambda_{i_t-1} \cup \{\varsigma_{i_t}\}$, update the reconstructed signal $\mathbf{y}_{i_t} = \mathbf{\Phi}_{\Lambda_{i_t}} \mathbf{\Phi}_{\Lambda_{i_t}}^{-1} \mathbf{y}$, and compute the residual $\mathbf{r}_{i_t} = \mathbf{y} - \mathbf{y}_{i_t}$;

Step 4. Go to step 2 if $i_t \leq s$, else terminate.

Next, based on the typical LO using the SFM and the OMP algorithm, the multiple intercepted mono-pulse radar signals' reconstruction is analyzed.

Firstly, according to the first two steps of the OMP algorithm, the purpose of step 2 in the first iteration is to find the atom that corresponds to the maximum of $|\langle \mathbf{\Phi}, \mathbf{y} \rangle|$. Hence, based on (9), it yields

$$\langle \mathbf{\Phi}, \mathbf{y} \rangle = \left[\begin{array}{cccc} \psi_M^H \mathbf{y} & e^{j\theta(m)} \psi_M^H \mathbf{y} & \cdots & e^{j(K-1)\theta(m)} \psi_M^H \mathbf{y} \end{array} \right]^T \tag{11}$$

In (11), the element $e^{jk\theta(m)} \psi_M^H \mathbf{y}$, $k = 0, 1, \cdots, K-1$ means the SFM demodulation and the discrete Fourier transform (DFT) in the kth NZ, which can be further expressed as:

$$e^{jk\theta(m)} \psi_M^H \mathbf{y} = \mathcal{F}_D \left[e^{jk \sin(2\pi f_{LO} m T_{ADC})} \sum_{i=1}^{s} A e^{2j\pi (f_i - k_i f_s) m T_{ADC} - j k_i \sin(2\pi f_{LO} m T_{ADC})} \right] \tag{12}$$

where $\mathcal{F}_D$ is the DFT operator. The result in (12) can be interpreted as the demodulation of the signal in each NZ by using the recover signal $r(m) = e^{jk \sin(2\pi f_{LO} m T_{ADC})}$, $k = 0, 1, \cdots, K-1$ and calculating the corresponding DFT results. The process in (12) is similar to the method that using the maximum peak value in frequency domain to estimate the NZ index k_i based on the SFM demodulation [13, 24].

Therefore, if the spectra of the outputs in (10) can be separated in frequency domain, the OMP algorithm can directly reconstruct these mono-pulse signals. However, because the multiple mono-pulse signals are unknown, it is possible to meet the situation in Fig. 2, and the completely frequency aliasing situation should be considered.

Under this condition, all folded signals in the 0th NZ have the same carrier frequencies, and the folded carrier frequencies are assumed as $f_{ci} = f_i - k_i f_s$, $i = 1, 2, \cdots, s$. Furthermore, (12) can be rewritten as

$$e^{jk\theta(m)} \psi_M^H \mathbf{y} = \mathcal{F}_D \left[e^{jk \sin(2\pi f_{LO} m T_{ADC})} \sum_{i=1}^{s} A e^{2j\pi f_{ci} m T_{ADC} - j k_i \sin(2\pi f_{LO} m T_{ADC})} \right] \tag{13}$$

According to (13), the element of $|\langle \mathbf{\Phi}, \mathbf{y} \rangle|$ in the kth NZ can be computed as

$$|\langle \mathbf{\Phi}, \mathbf{y} \rangle|(k) = |\mathcal{F}_D[y(m) r(m)]| = \left| A \sum_{i=1}^{s} \left\{ \mathcal{F}_D \left(e^{2j\pi f_{ci} m T_{ADC}} \right) * \mathcal{F}_D \left[e^{j(k-k_i) \sin(2\pi f_{LO} m T_{ADC})} \right] \right\} \right| \tag{14}$$

where * is the convolution. Since the DFT result is the spectrum discretization of the discrete-time Fourier transform (DTFT), the DTFT result is employed to approximate the DFT result in (14) to simplify the analysis. Besides, the impact of the window function on the signal $e^{2j\pi f_{ci} m T_{ADC}}$ is omitted to further simplify the analysis of (14). Thus, (14) can be computed as

$$\left|\mathcal{F}_D[y(m)r(m)]\right| \approx \left|A\sum_{i=1}^{s}\left\{2\pi\delta\left(f-f_{ci}\right) * \mathcal{F}_D\left[e^{j(k-k_i)\sin\left(2\pi f_{LO}mT_{ADC}\right)}\right]\right\}\right| \tag{15}$$

where $\delta(\cdot)$ is the impulse function, $f \in [-f_{ADC}/2,\ f_{ADC}/2)$ and $f_{ADC} = 1/T_{ADC}$.

Focusing on the second convolution term in (15), it can be calculated as

$$\begin{aligned}\mathcal{F}_D\left[e^{j(k-k_i)\sin\left(2\pi f_{LO}mT_{ADC}\right)}\right] &= \mathcal{F}_D\left[\sum_{p=-\infty}^{\infty} J_p(k-k_i)e^{j2\pi pf_{LO}mT_{ADC}}\right] \\ &\approx 2\pi\sum_{p=-\infty}^{\infty} J_p(k-k_i)\delta\left(f-pf_{LO}\right)\end{aligned} \tag{16}$$

where $J_p(\cdot)$ is the Bessel function with p order and the impact of the window function on $e^{j2\pi pf_{LO}mT_{ADC}}$ is also omitted. Substituting (16) into (15), it yields

$$\left|\left\langle\mathbf{\Phi},\mathbf{y}\right\rangle\right|(k) = \left|\mathcal{F}_D[y(m)r(m)]\right| \approx 4A\pi^2\left|\sum_{i=1}^{s}\sum_{p=-\infty}^{\infty} J_p(k-k_i)\delta\left(f-f_{ci}-pf_{LO}\right)\right| \tag{17}$$

If a single mono-pulse signal is intercepted, the maximum value of (17) is located in f_{c1} when $p=0$ and $k=k_1$, which means the NZ index of the modulated sampling scheme output is estimated and the signal can be directly reconstructed. According to the Bessel function, the maximum of (17) is

$$\left|\mathcal{F}_D[y(m)r(m)]\big|_{f=f_{c1},p=0,k=k_1}\right| \approx 4A\pi^2 J_0(0)\delta(0) = 4A\pi^2 \tag{18}$$

In terms of the multiple mono-pulse signals interception, the matched NZ index condition is considered firstly. The matched NZ index condition means the NZ index of the recover signal $r(m)$ equals the NZ index of one modulated sampling scheme output, and it can be expressed as $k=k_z$, $z \subset [1,2,\cdots,s]$. Therefore, the result in (17) is

$$\left|\mathcal{F}_D[y(m)r(m)]\big|_{k=k_z}\right| \approx 4A\pi^2\left|\sum_{z\neq i,i=1}^{s}\sum_{p=-\infty}^{\infty} J_p(k-k_i)\delta\left(f-f_{ci}-pf_{LO}\right) + 4A\pi^2\delta\left(f-f_{ci}\right)\right| \tag{19}$$

In (19), the result contains one peak that is located in $f=f_{ci}$. Focusing on this frequency, (19) can be rewritten as

$$\begin{aligned}\left|\mathcal{F}_D[y(m)r(m)]\big|_{k=k_z,p=0,f=f_{ci}}\right| &\approx 4A\pi^2\left|\left[\sum_{z\neq i,i=1}^{s} J_0(k-k_i)\delta(0)+\delta(0)\right]\right| \\ &= 4A\pi^2\left|\delta(0)\left[\sum_{z\neq i,i=1}^{s} J_0(k-k_i)+1\right]\right|\end{aligned} \tag{20}$$

In (20), when $f=f_{ci}$ and $k=k_z$, the signal with the matched NZ index meets its maximum whose value equals the result in (18), whereas the values of the rest signals in (20) with other NZ indices are smaller than the maximum value.

Furthermore, the unmatched NZ index situation is considered. The unmatched NZ index situation means the NZ index of the recover signal $r(m)$ is not equal to any NZ index of the output $y(m)$ (i.e., $k \neq k_z$). Similarly, the value of (17) in the frequency $f = f_{ci}$ is calculated like the analysis of (19) and (20). When $f = f_{ci}$ and $p = 0$, (17) can be expressed as

$$\left| \mathcal{F}_D[y(m)r(m)] \big|_{p=0, f=f_{ci}} \right| \approx 4A\pi^2 \delta(0) \left| \left[\sum_{i=1}^{s} J_0(k - k_i) \right] \right| \tag{21}$$

Compared with the summation terms in (20) and (21), it is possible that

$$\sum_{i=1}^{s} J_0(k - k_i) > \sum_{z \neq i, i=1}^{s} J_0(k - k_i) + 1 \tag{22}$$

The inequality in (22) means the value of the unmatched NZ index may be greater than the value of the matched NZ index when the LO modulation is the SFM. For example, two mono-pulse signals are considered. The first signal is in the 2$^{\text{nd}}$ NZ and the second signal is located in the 4$^{\text{th}}$ NZ. When the NZ index $k = 3$, this situation meets the expression in (21) and the summation term is $\sum_{i=1}^{2} J_0(1)$. When $k = 2$, this condition means the NZ index is matched and the summation term can be calculated as $J_0(2) + 1$ according to (20). Hence, we have $\sum_{i=1}^{2} J_0(1) > J_0(2) + 1$, and the result in (21) is greater than that in (20). Consequently, the return atom ς_1 in step 2 is located in the incorrect NZ.

The reason of the above phenomenon comes from the spectrum of the LO modulation that contains the Jacobi component. In other words, the SFM spectrum is not flat because it contains the summation of the Jacobi components in (17). Thus, maximum of $\left| \langle \mathbf{\Phi}, \mathbf{y} \rangle \right|$ in step 2 may located in the unmatched NZ.

Then, we continue to investigate the OMP algorithm. Since Λ_1 is the support consists of the return atom in step 2, the reconstructed signal in the first iteration can be computed as

$$\mathbf{y}_1 = \mathbf{\Phi}_{\Lambda_1} \mathbf{\Phi}_{\Lambda_1}^{-1} \mathbf{y} \tag{23}$$

where $\Lambda_1 \subset [0, \cdots, N-1]$. Because $\mathbf{\Phi}_{\Lambda_1}^{-1} = \mathbf{\Phi}_{\Lambda_1}^{H}$, $\mathbf{\Phi}_{\Lambda_1}^{-1} \mathbf{y}$ represents the spectrum peak value of $\mathbf{y}$ after the SFM demodulation that is located in the support Λ_1. The reconstructed signal spectrum in (23) is regarded as

$$\mathbf{y}_{rsp} = \Big[0 \ \cdots \ 0 \ \underset{\Lambda_1}{\underset{\uparrow}{\mathbf{\Phi}_{\Lambda_1}^{-1} \mathbf{y}}} \ 0 \ \cdots \ 0 \Big] \tag{24}$$

where $\mathbf{y}_{rsp} \in \mathbb{C}^N$. It can be interpreted that (24) is a narrowband filter and it only filters the spectrum in the support Λ_1. Besides, due to $\mathbf{\Phi}_{\Lambda_1}$ in (23) representing the SFM modulation and the IDFT of the filtered spectrum, (23) is the reconstructed signal in time domain corresponding to the support Λ_1.

When the support Λ_1 is located in the incorrect NZ, the reconstructed signal in (23) is another SFM signal. As a result, $\mathbf{r}_1 = \mathbf{y} - \mathbf{y}_1$ in step (3) will not clean any output of the modulated sampling scheme and it will add another SFM signal. Thus, under the completely frequency aliasing condition, the first iteration of the OMP algorithm fails to reconstruct any mono-pulse radar signals when the LO modulation type is the SFM.

4 Improved local oscillator modulation

According to the analysis in Sect. 3, the OMP algorithm fails to reconstruct the multiple mono-pulse signals in the completely frequency aliasing situation when the modulated sampling scheme uses the SFM LO. Meanwhile, because the atom calculation in the OMP algorithm is equivalent to the NZ index estimation method in [13], this method also fails to estimate the multiple NZ indices when the LO modulation is the SFM. Naturally, from the perspective of the receiving architecture, finding an improved LO modulation type to obtain a better multiple mono-pulse signals reconstruction is necessary to be investigated.

4.1 Improved local oscillator using periodic linear frequency modulation and reconstruction

In Sect. 3, the reason of the OMP algorithm failing to reconstruct the multiple mono-pulse signals under the completely frequency aliasing condition is that the SFM spectrum is out of flatness because of the Jacobi component. Considering the requirements of the modulated sampling scheme LO, the LO modulation type should be periodic and it should contain a certain bandwidth. Therefore, combining with the implementation of sample pulse train generation [25], the periodic linear frequency modulation (PLFM) is chosen as the improved LO modulation type and the LO of the modulated sampling scheme using the PLFM in (7) can be rewritten as

$$\theta_{PLFM}(m) = \pi \mu_0 \bmod (mT_{ADC},\ T_{LO})^2 \tag{25}$$

where μ_0 is the chirp rate, T_{LO} is the modulation period of the PLFM, $T_{LO} < T$ and mod means modulo. In (25), the instantaneous frequency is $2\pi\mu_0 \bmod (mT_{ADC},\ T_{LO})$ and it is linear in each period T_{LO}. According to the multiple intercepted mono-pulse radar signals in (1), the modulated sampling scheme in (2) and the LO modulation in (25), the outputs can be computed as

$$y(m) = A\sum_{i=1}^{s} e^{2j\pi(f_i - k_i f_s)mT_{ADC} - jk_i\pi\mu_0 \bmod (mT_{ADC},\, T_{LO})^2} \tag{26}$$

Then, the relation between the PLFM LO and the multiple mono-pulse signals reconstruction is analyzed. Based on the OMP algorithm, (12) and (25), the recover signal is

$$r_{PLFM}(m) = e^{jk\pi\mu_0 \bmod (mT_{ADC},\, T_{LO})^2} \tag{27}$$

where $k = 0, 1, \cdots, K-1$. The analysis of step 1 and step 2 of the OMP algorithm is like the analysis of (13). Focusing on the kth NZ, it yields

$$e^{jk\theta(m)}\psi_M^H\mathbf{y} = \mathcal{F}_D\left[Ae^{jk\pi\mu_0 \bmod (mT_{ADC},\, T_{LO})^2}\sum_{i=1}^{s} e^{2j\pi(f_i-k_if_s)mT_{ADC}-jk_i\pi\mu_0 \bmod (mT_{ADC},\, T_{LO})^2}\right] \tag{28}$$

Similar to the analysis in (14) and according to (28), the result of $\left|\langle\mathbf{\Phi},\mathbf{y}\rangle\right|$ in the k^{th} NZ is approximately expressed as:

$$\left|\langle\mathbf{\Phi},\mathbf{y}\rangle\right|(k) = \left|\mathcal{F}_D[y(m)r_{PLFM}(m)]\right| \approx \left|A\sum_{i=1}^{s}\left\{2\pi\delta(f-f_{ci}) * \mathcal{F}_D\left[e^{j(k-k_i)\pi\mu_0 \bmod (mT_{ADC},\, T_{LO})^2}\right]\right\}\right| \tag{29}$$

where $f_{ci} = f_i - k_i f_s,\ i = 1, 2, \cdots, s$. In (29), the DTFT result is also employed to approximate the DFT result, and the PLFM modulation part in (29) should be investigated to guarantee step 2 of the OMP algorithm returns the atom in the correct NZ under the completely frequency aliasing condition.

Focusing on the PLFM modulation part in (29), it can be calculated as

$$\mathcal{F}_D\left[e^{j(k-k_i)\pi\mu_0 \bmod (mT_{ADC},\, T_{LO})^2}\right] \approx \sum_{q=1}^{Q}\left|\xi_q(f)\right|e^{j\theta_q(f)} \tag{30}$$

where $\left|\xi_q(f)\right| = \frac{\sqrt{[C(u_{q1})+C(u_{q2})]^2+[S(u_{q1})+S(u_{q2})]^2}}{\sqrt{2(k-k_i)}}$,
$\theta_q(f) = \arctan\left[\frac{S(u_{q1})+S(u_{q2})}{C(u_{q1})+C(u_{q2})}\right] - \frac{\pi f^2}{(k-k_i)\mu_0}$, $q = 1, 2, \cdots, Q$, $Q = round\left(\frac{T}{T_{LO}}\right)$,
$M_{LO} = round\left(\frac{T_{LO}}{T_{ADC}}\right)$, $u_{q1} = \sqrt{2(k-k_i)\mu_0}\left[M_{LO}T_{ADC}(q-1) - \frac{f}{(k-k_i)\mu_0}\right]$,
$u_{q2} = \sqrt{2(k-k_i)\mu_0}\left[M_{LO}T_{ADC}q - \frac{f}{(k-k_i)\mu_0}\right]$,
$u_{Q2} = \sqrt{2(k-k_i)\mu_0}\left[M_{LO}T_{ADC} - \frac{f}{(k-k_i)\mu_0}\right]$, $C(\cdot)$ and $S(\cdot)$ are the Fresnel integral results.

In (30), the PLFM part in the frequency domain contains several Fresnel integral results and it approximates the summation of several rectangles, which means the spectrum of the PLFM has no Jacobi component and it is flat. According to the matched NZ index condition and the spectrum peak in (29), when $k = k_z$ and $f = f_{ci}$, the result in (29) is

$$\begin{aligned}\left|\mathcal{F}_D[y(m)r_{PLFM}(m)]\big|_{k=k_z, f=f_{ci}}\right| &\approx 2\pi A\left|\sum_{z\neq i, i=1}^{s}\left\{\delta(0) * \mathcal{F}_D\left[e^{j(k-k_i)\pi\mu_0 \bmod (mT_{ADC},\, T_{LO})^2}\right]\right\} + \delta(0)\right| \\ &= 2\pi A\left|\sum_{z\neq i, i=1}^{s}\sum_{q=1}^{Q}\left|\xi_q(0)\right|e^{j\theta_q(0)} + \delta(0)\right|\end{aligned} \tag{31}$$

In addition, the unmatched NZ index situation is considered, and the corresponding result in (29) is

$$\begin{aligned}\left|\mathcal{F}_D[y(m)r_{PLFM}(m)]\big|_{f=f_{ci}}\right| &\approx 2\pi A\left|\sum_{i=1}^{s}\left\{\delta(0) * \mathcal{F}_D\left[e^{j(k-k_i)\pi\mu_0 \bmod (mT_{ADC},\, T_{LO})^2}\right]\right\}\right| \\ &= 2\pi A\left|\sum_{i=1}^{s}\sum_{q=1}^{Q}\left|\xi_q(0)\right|e^{j\theta_q(0)}\right|\end{aligned} \tag{32}$$

Obviously, the maximum value in (31) is greater than that in (32) because (31) contains $\delta(0)$. Therefore, $\left|\mathcal{F}_D[y(m)r_{PLFM}(m)]\right|$ in (29) can achieve the maximum when $k = k_i$ and $f = f_{ci}$.

As a result, step 2 can obtain the support Λ_{i_t} that is located in the correct NZ. Furthermore, step 3 will demodulate, filter and clean the reconstructed signal. Finally, each intercepted signal can be reconstructed by the OMP algorithm. In the view of frequency analysis, compared with the spectrum of the SFM, the spectrum of the PLFM is flat due to the Fresnel integral, and the result of the matched NZ index in (31) will not be overwhelmed by the result of the unmatched NZ index in (32).

In terms of the parameter estimation or interception performance, when the result in (29) meets its maximum, the estimated NZ index and the folded carrier frequencies can be obtained as

$$\hat{k}_i, \hat{f}_{ci} = \underset{k_i, f_{ci}}{\arg} \left\{ \max \left[\left| \left\langle \mathbf{\Phi}, \mathbf{y} \right\rangle \right| (k) \right] \right\} \tag{33}$$

where $i = 1, 2, \cdots, s$. The estimated carrier frequencies of the intercepted multiple mono-pulse signals are computed as $\hat{f}_i = \hat{f}_{ci} + \hat{k}_i f_s$. Therefore, if the mono-pulse signals are recovered successfully, the parameters of the mono-pulse signals intercepted by the scheme can be estimated.

It is worth noting that the result of the last term in (30) will be no longer a rectangle when the distance between u_{q2} and u_{Q2} is very short. In other words, if $u_{Q2} - u_{q2}$ in (30) is very small, the linear frequency change of the last piece of the PLFM is not obvious and the corresponding spectrum is similar to the spectrum of single tone. Thus, the result in (30) will contain an impulse function, and the summation result in (32) is not flat, which may lead signal reconstruction failure. Since the parameters of the PLFM LO are known and the time domain of the mono-pulse signal can be obtained by signal detection [21], increasing the chirp rate or omitting the last piece of the PLFM in the modulated sampling scheme output can avoid this circumstance.

4.2 Modulation parameter setting criterion

Next, based on the improved LO modulation type, the parameter setting criterion is investigated to obtain a better reconstruction performance.

In this subsection, the CS model of the modulated sampling scheme $\mathbf{y} = \Phi\mathbf{X}$ in (2) is analyzed again. The sensing matrix $\mathbf{\Phi}$ satisfies the restricted isometry property (RIP) of order s with parameter $\delta_s \in [0,\ 1)$ if

$$(1 - \delta_s)\|\mathbf{X}\|_2^2 \leq \|\Phi\mathbf{X}\|_2^2 \leq (1 + \delta_s)\|\mathbf{X}\|_2^2 \tag{34}$$

holds for every s-sparse signal $\mathbf{X}$. Based on the relation between the RIP and eigenvalues [26], we have

$$1 - \delta_s \leq \lambda_{\min}[G(\mathbf{\Phi}_\Lambda)] \leq \lambda_{\max}[G(\mathbf{\Phi}_\Lambda)] \leq 1 + \delta_s \tag{35}$$

where the Gram matrix $G(\mathbf{\Phi}_\Lambda) = \mathbf{\Phi}_\Lambda^H \mathbf{\Phi}_\Lambda$, and $\mathbf{\Phi}_\Lambda$ consists of the columns of $\mathbf{\Phi}$ with indices $\Lambda \in s, s \subset \{1,\ 2,\ \cdots,\ N\}$.

Since the eigenvalues of the Gram matrix $G(\mathbf{\Phi})$ contain the eigenvalues information of all sub-matrix $\mathbf{\Phi}_\Lambda$, we focus on the Gram matrix $G(\mathbf{\Phi})$ [27] and it can be expressed as

$$G(\mathbf{\Phi}) = \begin{bmatrix} \mathbf{I}_M & \mathbf{G}_{10} & \cdots & \mathbf{G}_{(K-1)0} \\ \mathbf{G}_{01} & \mathbf{I}_M & \cdots & \mathbf{G}_{(K-1)1} \\ \vdots & \vdots & \ddots & \vdots \\ \mathbf{G}_{0(K-1)} & \mathbf{G}_{1(K-1)} & \cdots & \mathbf{I}_M \end{bmatrix} \tag{36}$$

In (36), $\mathbf{G}_{k1,k2} \in \mathbb{C}^{M\times M}$ is the off-diagonal sub-matrix, where the NZ indices are $k1 = 0,\ 1,\ \cdots,\ K-1$, and $k2 = 0,\ 1,\ \cdots,\ K-1$. According to the Gershgorin circle theorem, each Gershgorin disk radius should be less than δ_s to guarantee the sensing matrix $\mathbf{\Phi}$ satisfies the RIP because the diagonal elements of $G(\mathbf{\Phi})$ are equal to 1. Thus, the off-diagonal element in the off-diagonal sub-matrix is [17]

$$\left| g_{k1,k2,c,r}\big|_{k1\neq k2} \right| < \frac{\delta_s}{s} \tag{37}$$

where the column index is $c = 0,\ 1,\ \cdots,\ M-1$ and the row index is $r = 0,\ 1,\ \cdots,\ M-1$. If the number of s-sparse signals increases, the values of off-diagonal elements should be decreased to guarantee the relation in (37).

Then, the off-diagonal element in (36) can be calculated as

$$g_{k1,k2,c,r} = \frac{1}{M}\sum_{m=0}^{M-1} e^{j(k2-k1)\theta_{PLFM}(m)} e^{-j\frac{2\pi}{M}m(r-c)} \tag{38}$$

The off-diagonal element in (38) can be regarded as the DFT result of the signal using the improved LO modulation. Therefore, to recover more s-sparse signals intercepted by the modulated sampling scheme (i.e.. increasing s), the bandwidth of the LO modulation B_{LO} should be increased to satisfy (37), which means the chirp rate μ_0 or the modulation period in (25) should be greater.

Moreover, the above criterion can be interpreted in frequency domain as well. According to the Parseval theorem, when the bandwidth of the LO modulation increases, the spectrum magnitude of the LO modulation will decrease and the frequency aliasing impact is less. However, increasing the bandwidth of the LO modulation has a limitation because the modulated sampling scheme requires $B_{LO} \ll f_s$ [23].

Furthermore, since the modulated sampling is in the middle of the uniform sampling and the CS random sampling, the statistical RIP (StRIP) is employed to analyze the parameter setting criterion. The upper bound on general RIP numbers of the modulated sampling scheme is [11]

$$\delta_s \leq sC\sqrt{\frac{1}{B_{LO}T}} \tag{39}$$

where C is a constant related to the LO modulation type and the LO modulation bandwidth. Therefore, when the number of the intercepted mono-pulse signals increases (i.e., s increases), the LO modulation bandwidth B_{LO} should be increased to guarantee the relation in (39). On the other hand, when B_{LO} increases, the upper bound in (39) will be decreased and δ_s can satisfy the recovery requirement $\delta_{2s} < \sqrt{2}-1$ [28].

In summary, compared with the typical LO modulation type using the SFM, the OMP algorithm has the ability to reconstruct the multiple mono-pulse radar signals intercepted by the modulated sampling scheme using the PLFM LO under the completely frequency aliasing condition. Besides, increasing the PLFM bandwidth can increase the reconstruction number of the multiple mono-pulse radar signals.

4.3 Extended discussion

To further explain the improvement of the PLFM LO, some other modulation types of the LO are discussed. In terms of the LO modulation requirements [11–13], the LO modulation should have a bandwidth and be periodic. The LO modulation bandwidth is the information to recover the original signal frequency and its value is required to be distinguishable in different NZs. Moreover, because the sample pulse is generated at the ZCR time, the LO modulation should be periodic for the purpose of sample pulse generation implementation. In addition, the LO modulation is non-random to preserve the intercepted signal structure. Presently, the main non-random periodic modulation types are the phase modulation and the frequency modulation. Hence, the binary phase shift keying (BPSK) and the periodic nonlinear frequency modulation (PNLFM) are considered in this subsection.

When the LO modulation type is the BPSK, the ZCR time is calculated by the summation of several BPSK signals with different carrier frequencies and BPSK codes [29]. Essentially, this LO modulation can be regarded as a receiving structure using multiple channels with different codes like the MWC [7], whereas the merit of the modulated sampling scheme using single channel is vanished and it brings more receiving cost.

Then, the LO using the PNLFM is discussed, and the LO of the modulated sampling scheme using the cubic PNLFM can be expressed as

$$\theta_{PNLFM}(m) = 2\pi \left[\frac{\mu_1 \bmod (mT_{ADC},\ T_{LO})^2}{2} + \frac{\mu_2 \bmod (mT_{ADC},\ T_{LO})^3}{3} \right] \tag{40}$$

where μ_1 and μ_2 are the modulation parameters of the quadratic and cubic terms, respectively. Other parameters in (40) are the same as those in (25).

The cubic term in (40) can be regarded as parts of Maclaurin series of sin and cos functions with the independent variable μ_2. As a result, the spectrum of the PNLFM is not as flat as the PLFM. Thus, according to the analysis in Sect. 4.1, the multiple signals reconstruction performance using the PNLFM LO will be deteriorated.

Furthermore, compared with the PNLFM, the ZCR time generation and the implementation of the PLFM are easier because of the linear frequency property. Moreover, since the PLFM in one period has an optimum kernel function—fractional Fourier transform (FRFT) [30] and it is a linear transform, the output of the modulated sampling scheme using PLFM LO can be processed easily. Overall, this paper chooses the PLFM as the LO modulation to improve the multiple mono-pulse reconstruction.

5 Experiments

In this section, several simulation experiments are given to prove the analysis in this paper.

5.1 Multiple mono-pulse signals reconstruction using typical and improved local oscillator modulations

Firstly, the typical modulated sampling scheme using the SFM LO is considered. The LO carrier frequency is 1 GHz, the LO modulation frequency f_{LO} is 20 MHz, the SFM modulation coefficient is 1 and the number of the NZs is 10.

Two groups of multiple mono-pulse radar signals are used as the intercepted signals. The signals in the first group are assumed as $x_1(t) = \sum_{i=1}^{2} A_i e^{2j\pi f_i t + j\varphi_i}$, where the signal carrier frequencies are 2.21 GHz and 4.24 GHz, the signal amplitudes A_i are all equal to 1, the signal durations are 0.5 μs and the initial phases φ_i are 0. The second group is $x_2(t) = \sum_{i=3}^{4} A_i e^{2j\pi f_i t + j\varphi_i}$, where the signal carrier frequencies are 2.21 GHz and 4.21 GHz, and other parameters are the same as those in the first group. The mono-pulse radar signals in the two groups are in S band and C band. The signal reconstruction method is the OMP and the number of the iterations is 3. Based on the modulated sampling scheme, Fig. 3 shows the spectra of the intercepted signals in the two groups and the corresponding spectra of the reconstructed signals.

Figure 3a demonstrates the spectra of the first group. The spectra of the two intercepted signals and the reconstructed signals are all located in the same frequency. Thus, the reconstruction using the OMP algorithm for the first group is success. Figure 3b is the spectra of the second group and it can be seen that the spectra of the two intercepted signals and the reconstructed signals are different, which implies the OMP algorithm fails to reconstruct the intercepted signals. In detail, according to (10), the folded carrier frequencies in the first group can be computed as 0.21 GHz and 0.24 GHz. Therefore, the two folded signals are partly frequency aliasing and the OMP algorithm can reconstruct these signals. However, the folded carrier frequencies in the second group all

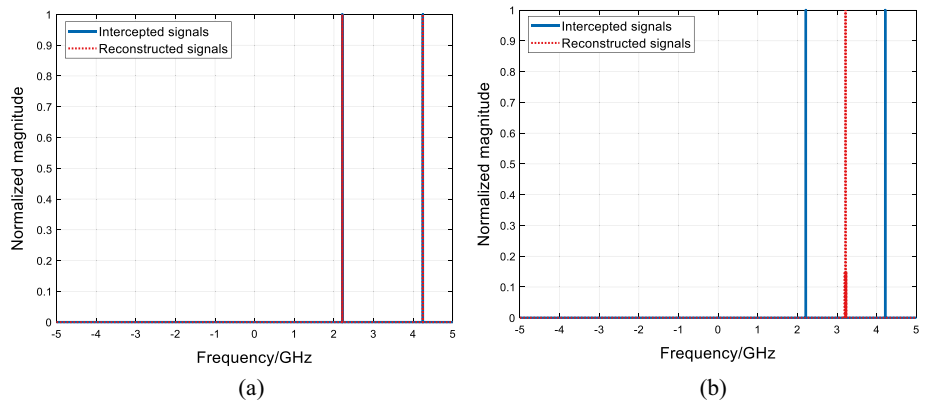

Fig. 3 Spectra of intercepted mono-pulse signals and reconstructed signals using SFM LO. **a** First group, **b** Second group

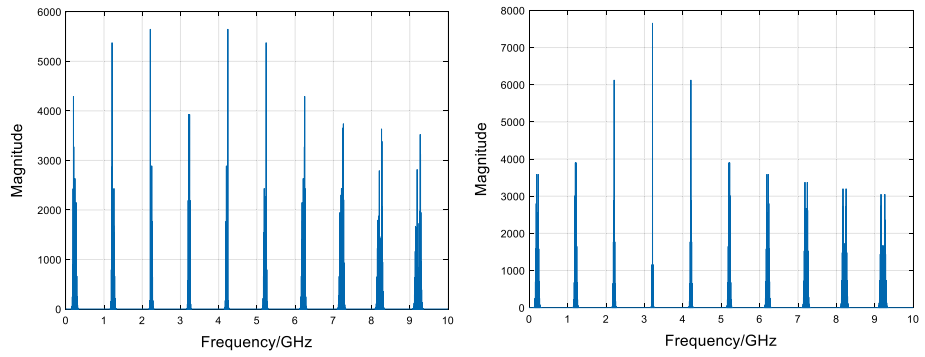

Fig. 4 Step 2 results of OMP algorithm in the first iteration. **a** First group, **b** Second group

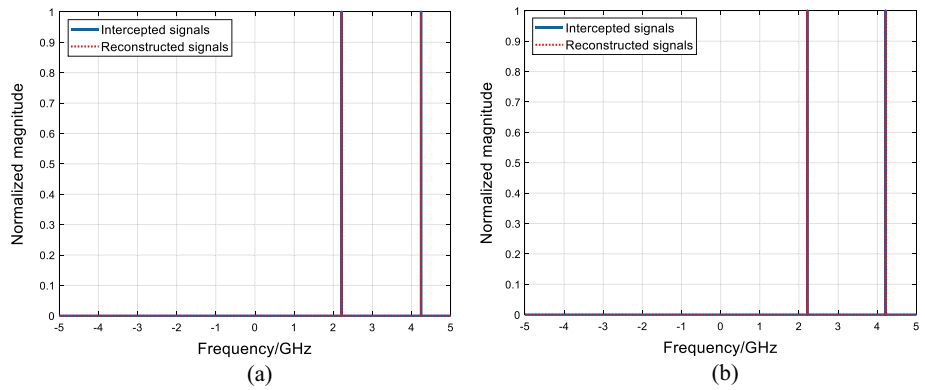

Fig. 5 Spectra of intercepted mono-pulse signals and reconstructed signals using PLFM LO. **a** First group, **b** Second group

equal 0.21 GHz, and these folded signals are completely frequency aliasing. Under this circumstance, the OMP algorithm fails to reconstruct the multiple mono-pulse signals.

Then, to further explain the results in Fig. 3 and prove the analysis in Sect. 3, Fig. 4 gives the step 2 results of the OMP algorithm in the first iteration when the two groups of multiple mono-pulse signals are intercepted by the modulated sampling scheme.

Considering the carrier frequencies of the signals in each group, the NZ indices of the two signals can be computed as 2 and 4, respectively. According to the above parameters, the NZ bandwidth is 1 GHz. As shown in Fig. 4a, the maximum peaks are located in the 2nd and the 4th NZs, and they can return the atoms in the correct NZs. However, the maximum peak in Fig. 4b is in the 3rd NZ, which implies that the return atom is located in the incorrect NZ. Therefore, the OMP algorithm fails to reconstruct to the multiple signals in the second group.

Furthermore, the improved LO modulation using the PLFM is considered. The chirp rate is 181 MHz/μs, the modulation period of the PLFM is 0.13 μs and other parameters of the modulated sampling scheme are the same as those in Fig. 3. The two groups of the mono-pulse signals in Fig. 3 are also used as the intercepted signals. Figure 5 shows the spectra of the intercepted signals and the reconstructed signals.

As shown in Fig. 5, the two groups of multiple mono-pulse signals are all reconstructed successfully when the LO modulation is the PLFM. Particularly, compared with the reconstruction result in Fig. 3b, Fig. 5b shows that the OMP algorithm can reconstruct the completely frequency aliasing folded signals. Therefore, the improved LO is a better choice for the multiple mono-pulse signals reconstruction.

5.2 Reconstruction performance analysis

Next, the reconstruction performances for multiple mono-pulse radar signals are given based on the modulated sampling scheme. In this subsection, the reconstruction probability for the multiple mono-pulse signals is defined as

$$P_r = \frac{N_{\text{correct}}}{N_{\text{total}}} \tag{41}$$

where N_{correct} is the number of successful reconstruction experiments and N_{total} is the number of total Monte Carlo simulations. The successful reconstruction means each mono-pulse signal in one group is reconstructed correctly. Based on the analysis in Sect. 4, if each mono-pulse signal can be reconstructed, the parameters of the intercepted signals can be directly obtained. Therefore, the reconstruction probability P_r equals the parameter estimation performance of the interception system.

The two groups of mono-pulse signals in Fig. 3 are used. Two LO modulation types of the modulated sampling scheme are employed, and they are the SFM and the PLFM. The parameters of the modulated sampling scheme using the SFM LO are the same as those in Fig. 3 and the parameters of the PLFM LO are the same as those in Fig. 5. The input noise is the white Gaussian noise. The input signal-to-noise ratio (SNR) is from -15 dB to 5 dB, and 500 Monte Carlo experiments are conducted for each SNR. The reconstruction method is the OMP algorithm, and the iteration number of the OMP algorithm is 3.

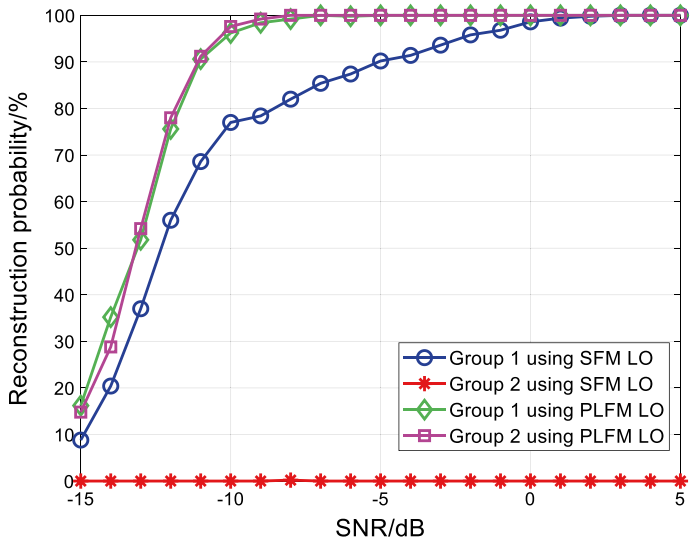

Fig. 6 Reconstruction probabilities of signals in two groups

Figure 6 demonstrates the reconstruction probabilities of the two groups using the two LO modulation types.

In Fig. 6, when the SNR is greater than -5 dB, the reconstruction probability of the two mono-pulse signals in group 1 using the SFM LO can reach 90%. In the meantime, the reconstruction probability of group 2 using the SFM LO is always around 0%, which means the OMP algorithm using the SFM LO fails to reconstruct the two mono-pulse signals in group 2. This result coincides with the analysis of Sect. 3 and Fig. 3. However, the OMP algorithm using the PLFM LO can reconstruct the both groups. In detail, when the SNR is higher than -11 dB, the reconstruction probabilities of the two groups can achieve 90%. Moreover, focusing on the reconstruction performance of group 1, the performance using the PLFM LO is better than that using the SFM LO. The reasons are that the PLFM LO has a larger bandwidth and its spectrum is flat, which decreases the frequency aliasing impact.

In addition, considering the different number of s-sparse mono-pulse signals and the PLFM LO, the corresponding reconstruction probabilities are simulated. Three groups of mono-pulse signals are assumed as the intercepted signals. The signals in group 1 can be written as

$$x_1(t) = \sum_{i=1}^{2} A_i e^{2j\pi f_i t + j\varphi_i} \tag{42}$$

where $A_i = 1,\ i = 1, 2,\ f_1 = 1.21$ GHz, $f_2 = 2.21$ GHz, $\varphi_i = 0,\ i = 1, 2$ and the signal durations $T = 0.5\ \mu s$.

The signals in group 2 are:

$$x_2(t) = \sum_{i=3}^{5} A_i e^{2j\pi f_i t + j\varphi_i} \tag{43}$$

where $A_i = 1,\ i = 3, 4, 5,\ f_3 = 1.21$ GHz, $f_4 = 2.21$ GHz, $f_5 = 3.21$ GHz, $\varphi_i = 0,\ i = 3, 4, 5$ and the signal durations $T = 0.5\ \mu s$.

The signals in group 3 can be expressed as:

$$x_3(t) = \sum_{i=6}^{10} A_i e^{2j\pi f_i t + j\varphi_i} \tag{44}$$

where $A_i = 1,\ i = 6, \cdots, 10,\ f_6 = 1.21$ GHz, $f_7 = 2.21$ GHz, $f_8 = 3.21$ GHz, $f_9 = 4.21$ GHz, $f_{10} = 0.21$ GHz, $\varphi_i = 0,\ i = 6, \cdots, 10$ and the signal durations $T = 0.5\ \mu s$.

As to the modulated sampling schemes, three PLFM LOs are used. The chirp rate of the first LO is 80 MHz/μs, the chirp rate of the second LO is 150 MHz/μs, and the chirp rate of the third LO is 180 MHz/μs. Other parameters of the modulated sampling schemes are the same as those in Fig. 5. The input SNR is from -10 dB to 10 dB and 500 Monte Carlo experiments are conducted for each SNR. The iteration number of the OMP algorithm is 6. Figure 7 gives the reconstruction probability of each group based on the three LOs.

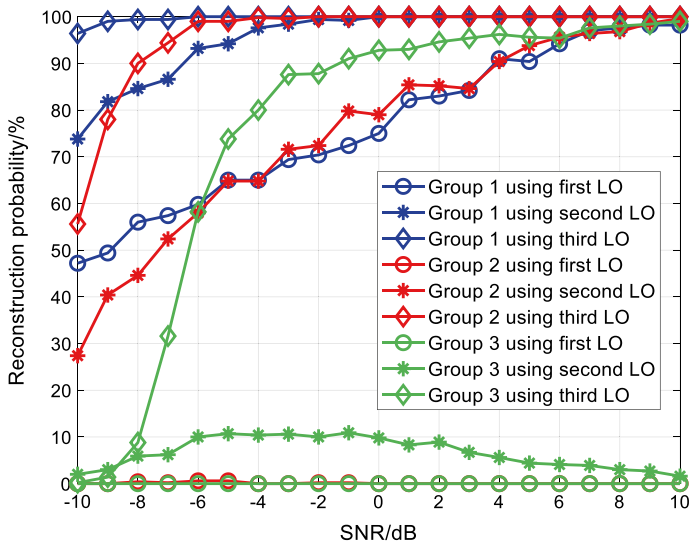

Fig. 7 Reconstruction probabilities of multiple signals using different LO bandwidths

According to the parameters of the intercepted signals and the modulated sampling scheme, the folded carrier frequencies of the signals in the three groups are equal to 0.21 GHz, which means these outputs are all completely frequency aliasing.

As illustrated in Fig. 7, the reconstruction probabilities of group 1 using three LOs can reach 90% when the SNR is higher than 4 dB. In detail, the probability of group 1 using the first LO is worse than the probabilities of other two LOs, and the performance of group 1 using the third LO is the best. The reason is that the third LO has a larger bandwidth, which brings a better reconstruction result. Besides, the probability of group 2 using the first LO is around 0% and the OMP algorithm fails to reconstruct these signals. However, the OMP algorithm using the second and the third LOs can reconstruct the three signals in group 2 when the SNR is greater than 4 dB, and the performance using the third LO is better than the second LO. Furthermore, the five signals in group 3 can be reconstructed by using the third LO and other LOs fail to reconstruct them. In addition, the probability fluctuation of group 3 using the second LO comes from the noise.

The results in Fig. 7 show that expanding the LO modulation bandwidth can improve the OMP algorithm reconstruction probability when the number of s-sparse signals increases, which proves the analysis in Sect. 4.2. Specifically, when the LO modulation type is the PLFM, the OMP algorithm can reconstruct the s-sparse mono-pulse signals intercepted by the modulated sampling scheme even the folded outputs are completely frequency aliasing.

Finally, two LO modulation types are considered, and they are the PLFM and the PNLFM. The parameters of the modulated sampling scheme using the PLFM LO are the same as those using the third LO in Fig. 7. In terms of the modulated sampling scheme using the PNLFM LO, two LOs with different bandwidth are employed. The quadratic and cubic modulation parameters of the first PNLFM LO are 150 MHz/μs and 0.235 GHz/μs^2. The quadratic and cubic modulation parameters of the second PNLFM LO are 150 MHz/μs and 0.35 GHz/μs^2. Other parameters of the two modulated

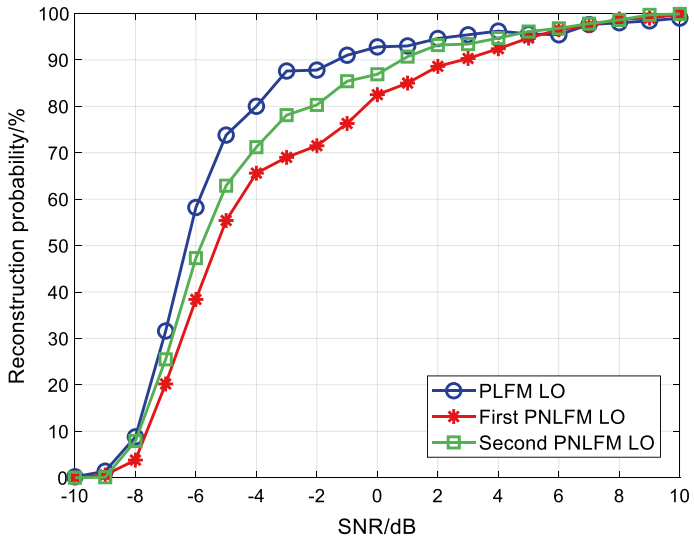

Fig. 8 Reconstruction probabilities using different LO modulation types

sampling schemes are the same as those in Fig. 5. The signals in group 3 in (44) are the intercepted signals. Figure 8 demonstrates the reconstruction probability using different LO modulation types.

In Fig. 8, the reconstruction probability using the PLFM LO is great than 90% when the SNR is greater than − 2 dB, whereas the reconstruction probability using the first PNLFM LO can reach the same performance when the SNR is larger than 2 dB. According to the parameter settings, the bandwidths of the two PNLFM in one period are 23.472 MHz and 25.415 MHz, respectively. The bandwidth of the PLFM in one period is 23.4 MHz. Hence, when the bandwidths are almost the same, the reconstruction performance using the PLFM LO is better than that using the first PNLFM LO in Fig. 8. Meanwhile, the performance using the second PNLFM LO is better than that using the first PNLFM LO since the bandwidth of the second PNLFM in one period is larger. However, it is still worse than the performance using the PLFM LO, which proves the analysis in Sect. 4.3.

6 Results and discussion

According to the above experiments, it can be seen that the modulated sampling scheme using the typical SFM LO fails to reconstruct multiple mono-pulse signals under the completely frequency aliasing condition, which is shown in Fig. 3. The reason of this failure is the SFM spectrum containing Jacobi component that is analyzed in Sect. 3, and the experiment results in Fig. 4 prove it. Then, the modulated sampling scheme using the PLFM LO can reconstruct multiple mono-pulse signals in the completely frequency aliasing situation, and it can be seen in Fig. 5. Moreover, the results in Fig. 6 prove the effectiveness of the improved LO modulation. Furthermore, the results in Fig. 7 demonstrate the analysis of the LO modulation parameter setting. At last, combing with other modulation type, the simulations in Fig. 8 show that the PLFM is a better choice for multiple mono-pulse signals reconstruction.

In summary, when the multiple mono-pulse signals are intercepted by the modulated sampling scheme using the PLFM LO, the OMP algorithm can reconstruct the folded signals under the completely frequency aliasing condition, which overcomes the drawback of the typical modulated sampling scheme. Although the LO modulation can also use other modulation types, the PLFM LO is still a better choice to improve the reconstruction performance. The future works include the optimal modulation type discussion in different receiving applications and investigating the wideband signal reconstruction using the improved LO modulation.

7 Conclusion

In this paper, the relation between the LO modulation of the modulated sampling scheme and the multiple mono-pulse radar signals reconstruction using the OMP algorithm is investigated. The sampling and the signal model are given firstly. The folded outputs are analyzed and the completely frequency aliasing situation is considered. Then, combining with the modulated sampling scheme model, the reason that the OMP algorithm using the typical SFM LO fails to reconstruct the multiple mono-pulse signals under the completely frequency aliasing condition is analyzed mathematically. Furthermore, the improved LO using the PLFM is given and its effectiveness of reconstruction multiple mono-pulse signals is proved. Additionally, the parameter setting criterion of the PLFM LO is given to improve the reconstruction number of the multiple mono-pulse signals and other choices of the LO modulation types are discussed. At last, several simulations are conducted to prove the analysis, and the improved LO modulation can reconstruct multiple mono-pulse signals under the completely frequency aliasing condition.

Abbreviations

LO: Local oscillator; PLFM: Periodic linear frequency modulation; RIP: Restricted isometry property; SFM: Sinusoidal frequency modulation; ZCR: Zero-crossing rising; ADC: Analog-to-digital converter; SNR: Signal-to-noise ratio; DFT: Discrete Fourier transform; BPSK: Binary phase shift keying; NYFR: Nyquist folding receiver; ADC: Analog-to-digital converter; CS: Compressive sensing; OMP: Orthogonal matching pursuit; RF: Radio frequency; NZ: Nyquist zone; FRFT: Fractional Fourier transform; DTFT: Discrete-time Fourier transform; PNLFM: Periodic nonlinear frequency modulation.

Acknowledgements

The authors thank the reviewers for their comments.

Authors' contributions

ZQ is the first author of this paper. His main contributions include the basic idea, mathematical analysis, derivation, simulations, and writing. MS is the second author and the corresponding author. His contribution is refining and administration. JZ is the third author, and his contribution is the basic idea analysis. XT is the fourth author, and his contribution is simulation check. HS is the fifth author, and her contribution is grammar check. All authors read and approved the final manuscript.

Funding

This research was funded by the National Natural Science Foundation of China (Grant No. 61901149, No. 61906055, No. 62101167), and Characteristic Discipline Development Project (Grant No. JCKY2019415D002).

Availability of data and materials

Not applicable.

Declarations

Competing interests

The authors declare that they have no competing interests.

Author details

[1]School of Communication Engineering, Hangzhou Dianzi University, Hangzhou, People's Republic of China. [2]Guoke Dianlei (Beijing) Electronic Equipment Technology Co. Ltd, Chengdu, People's Republic of China.

Received: 24 November 2021 Accepted: 1 March 2022
Published online: 18 March 2022

References

1. D. Lynch, *Introduction to RF Stealth* (SciTech Publishing Inc., Raleigh, 2004)
2. O. Holt, Technology survey: a sampling of ELINT receivers. J. Electronic Defense **38**(8), 35–43 (2015)
3. J. Tsui, C. Cheng, *Digital Techniques for Wideband Receivers*, 3rd edn. (SciTech Publishing, Danvers, 2015)
4. G. Valley, Photonic analog-to-digital converters. Opt. Express **15**(5), 1955–1982 (2007)
5. A. Bhandari, F. Krahmer, R. Raskar, Unlimited Sampling of Sparse Sinusoidal Mixtures. IEEE International Symposium on Information Theory, Vail, CO, USA (2018).
6. K. Sami, L. Jason, W. Michael, et al., Analog-to-information conversion via random demodulation, in *IEEE Dallas/CAS Workshop on Design, Applications, Integration and Software*, Richardson, TX, USA (2006).
7. M. Mishali, Y. Eldar, A. Elron, Xampling: signal acquisition and processing in union of subspaces. IEEE Trans. Signal Process. **59**(10), 4719–4734 (2011)
8. J. Tropp, J. Laska, M. Duarte et al., Beyond Nyquist: efficient sampling of sparse, band-limited signals. IEEE Trans. Inf. Theory **56**(1), 520–544 (2010)
9. K. Jiang, Y. Xiong, B. Tang, Wideband spectrum sensing via derived correlation matrix completion based on generalized coprime sampling. IEEE Access **7**, 117403–117410 (2019)
10. K. Sujit, M. Anamitra, Signal recovery from random measurements via extended orthogonal matching pursuit. IEEE Trans. Signal Process. **63**(10), 2572–2581 (2015)
11. R. Maleh, G. Fudge, RIP analysis of modulated sampling schemes for recovering spectrally sparse signals. arXiv:1207.7347v1, Available: arXiv.com (2012).
12. M. Ray, L. Gerald, L. Fudge et al., Analog-to-information and the Nyquist folding receiver. IEEE J. Emerg. Sel. Top. Circuits Syst. **2**(3), 564–578 (2012)
13. D. Zeng, H. Cheng, J. Zhu et al., Parameter estimation of LFM signal intercepted by synchronous Nyquist folding receiver. Prog. Electromagn. Res. C **23**, 69–81 (2011)
14. T. Li, Q. Zhu, Z. Chen, Parameter estimation of SAR signal based on SVD for the Nyquist folding receiver. Sensors **18**, 16 (2018)
15. T. Gong, Z. Liu, C. Xie et al., Property investigation on the additive white Gaussian noise after sub-Nyquist sampling. IEEE Access **4**, 1–7 (2016)
16. T. Li, Q. Zhu, X. Fan, Z. Chen, Parameter estimation of LFM signal intercepted by improved dual-channel Nyquist folding receiver. Electron. Lett. **54**(10), 659–661 (2018)
17. K. Jiang, S. Chen, B. Tang, The RIP and block-RIP analysis of Nyquist folding receiver for recovering signals. EURASIP J. Adv. Signal Process. 92 (2016).
18. H. Rong, Q. Chen, Research on jamming efficiency and measures against mono-pulse radar, in *IEEE Advanced Information Technology, Electronic and Automation Control Conference*, Chongqing, China, pp. 883–886, (2015).
19. Z. Qiu, P. Wang, J. Zhu et al., Estimation of both Nyquist zone index and code rate for BPSK radar signal intercepted by Nyquist folding receiver. IET Radar Sonar Navig. **11**(11), 1652–1663 (2017)
20. J. Martin, Analysis of the Nyquist folding receiver. Master thesis, University of Oklahoma (2018).
21. Z. Qiu, P. Wang, J. Zhu et al., NYFR output pulse radar signal TOA analysis using extended Fourier transform and its TOA estimation. J. Syst. Eng. Electron. **28**(2), 212–223 (2017)
22. E. Candes, J. Romberg, T. Tao, Robust uncertainty principles: exact signal reconstruction from highly incomplete frequency information. IEEE Trans. Inf. Theory **52**(2), 489–509 (2006)
23. G. Fudge, R. Bland, M. Chivers, et al, A Nyquist folding analog-to-information receiver, in *The 42nd Asilomar Conference on Signals, Systems and Computers*, Pacific Grove, pp. 541–545 (2008).
24. Z. Qiu, P. Wang, M. Sun et al., Parameter estimation of frequency shift keying radar signal intercepted by Nyquist folding receiver using periodic linear frequency modulation local oscillator. IET Radar Sonar Navig. **15**(9), 1–15 (2021)
25. Z Xia, Z Zhao, T Zhang, et al., A novel method of space-borne cognitive SAR signal generation based on FPGA and DDS, in *IET International Radar Conference, Online Conference*, 2020.
26. W. Dai, O. Milenkovic, Subspace pursuit for compressive sensing signal reconstruction. IEEE Trans. Inf. Theory **55**(5), 2230–2249 (2009)
27. J. Haupt, L. Applebaum, R. Nowak, On the restricted isometry of deterministically subsampled Fourier matrices, in *The 44th Annual Conference on Information Sciences and Systems*, Princeton, NJ, USA, 1–6 (2010).
28. E. Candès, The restricted isometry property and its implications for compressed sensing. C.R. Math. **346**(9–10), 589–592 (2008)
29. X. Zeng, D. Zeng, H. Cheng et al., Intercept of frequency agile signals with Nyquist folding receiver using binary phase shift keying as the local oscillator. IETE J. Res. **58**(1), 44–49 (2014)
30. R. Tao, F. Zhang, Y. Wang, Research progress on discretization of fractional Fourier transform. Sci. China **51**(7), 859–880 (2008)

Publisher's Note